ECOLOGY

# Global spatiotemporal patterns of demographic fluctuations in terrestrial vertebrates during the Late Pleistocene

**Zitian Li[1,2,3]†, Huizhong Fan[1]†, Ziyan Liao[4]†, Yuxuan Wang[1], Fuwen Wei[1,2,3]***



**Demographic fluctuations are crucial for assessing species' threat levels, yet their global spatiotemporal patterns and historical drivers remain unknown. Here, we used single whole-genome sequence data for 527 extant and widespread terrestrial vertebrates to investigate their demographic fluctuations during the Late Pleistocene. Effective population size ($N_e$) simulations indicated that all taxa experienced a population decline from the Last Interglacial to the Last Glacial Maximum (LGM). After the LGM, birds and amphibians underwent population expansion, whereas mammals and reptiles' populations declined. Regions with high $N_e$ shifted from Neotropical to Afrotropical and to Palearctic, some overlapping with recognized glacial refugia and biodiversity hotspots. In addition, climate-related factors exerted long-term effects on $N_e$, while human disturbances might confine to specific regions around the Pleistocene-Holocene boundary. This study underscores the significance of quantifying vertebrate genetic vulnerability to guide biodiversity conservation in response to environmental changes.**

## INTRODUCTION

Global biodiversity is facing serious challenges, and the rate of species extinction is rapidly increasing (*1*). Demographic decline, driven by marked climate change and human disturbance, is considered a primary factor in the biodiversity crisis (*2*, *3*). Exploring historical demographic dynamics of species and the underpinning mechanisms can offer valuable insights into species' adaptability and resilience in response to environmental changes during the Anthropocene, which can help inform conservation policy and practice (*4*). Genomics-based meta-analysis—particularly that involving the analysis and simulation of effective population size ($N_e$), a key parameter for assessing the evolutionary potential and long-term survival of species (*5*, *6*)—is among the most effective strategies for investigating historical demographic fluctuations.

The Late Pleistocene [~129.0 to 11.7 calibrated thousand years (ka) before the present] is characterized by a megafauna extinction event, which substantially affected the contemporary biodiversity (*7*). Archeological evidence suggests that, during this period, terrestrial vertebrates, particularly megafauna, experienced a severe population decline and a global-scale extinction event (*8*). However, because of the existence of climatic refuges and the differentiation of species' life-history traits, it is expected that not all the taxa followed a consistent population-changing pattern in this geological period (*9*). For example, previous $N_e$-based genomic meta-analyses showed that, although numerous species, particularly extant megafauna, exhibited demographic decline during the Late Pleistocene (*10*–*14*), certain species could present upward population trends, such as *Arctocephalus gazella* (*15*) and *Macaca fascicularis* (*16*). A research based on 263 genomes demonstrated highly diverse demographic histories of birds during the Pleistocene, generally categorized into seven distinct patterns (*4*). This implied that a comprehensive genomics-based assessment on the demographic fluctuations of all terrestrial vertebrate groups is needed.

At the spatial level, because of geographic effect and regional climatic variability, population fluctuations should be asynchronous across the globe. Unfortunately, there is little information on the geographic patterns of demographic histories of species in literature. Recent genomic data indicate that before 32 to 76 ka, Africa and Eurasia experienced megafauna population declines, while Australasia and the Americas could have stable and positive growth (*13*, *17*). Another study on killer whales found that high-latitude populations of global ocean basins experienced a decline in $N_e$ during the Last Glacial Period (LGP; ~115 to 11.7 ka) (*18*). Despite this evidence, it is of great values to provide a global mapping on the spatial $N_e$ distribution in terrestrial vertebrates, analyze $N_e$'s biogeographic patterns, and explore potential latitudinal gradients during the Late Pleistocene. These $N_e$ spatial analyses could clarify the different responses of terrestrial vertebrates distributed in different global regions to cold climates.

Climate change and human influence are widely regarded as the primary drivers of demographic species fluctuations during the Late Pleistocene (*13*, *19*). Climate change, generally reflected in the ice age cycles of this period, reduces the availability of suitable habitats, thus exacerbating population decline throughout glacial periods (*20*). Additionally, human overkill is another plausible factor, because larger-sized animals are the preferential exploitation targets, and their local extinction often coincides with human arrival (*19*). An integrative analysis of genomic data indicated that the megafauna population decline during the Late Pleistocene was due more to the global expansion of humans than climatic shifts (*13*). However, the effects of climate change and human disturbance on all terrestrial vertebrates remain unclear, particularly regarding geographical heterogeneity.

Here, we reconstructed the population histories and estimated the suitable distributions for 527 terrestrial vertebrates during the Late Pleistocene, so as to provide one of the most holistic analyses on the global spatiotemporal patterns of 527 extant and widespread terrestrial vertebrates. We examined the role of key variables related to the inherent characteristics of terrestrial vertebrates as well as abiotic and biotic factors, to explain these patterns, and tested the following

[1]CAS Key Laboratory of Animal Ecology and Conservation Biology, Institute of Zoology, Chinese Academy of Sciences, Beijing 100101, China. [2]Jiangxi Key Laboratory of Conservation Biology, College of Forestry, Jiangxi Agricultural University, Nanchang 330045, China. [3]University of Chinese Academy of Sciences, Beijing 100049, China. [4]Chengdu Institute of Biology, Chinese Academy of Sciences, Chengdu 610213, China.
*Corresponding author. Email: weifw@ioz.ac.cn
†These authors contributed equally to this work.

three hypotheses: (i) terrestrial vertebrate populations should consistently decline during the ice age; (ii) spatiotemporal $N_e$ patterns would vary across zoogeographic realms, with a likely latitudinal gradient, and that regions with the highest $N_e$ would shift over time in response to the species' range and climate change; and (iii) climate and human disturbances jointly determined the global $N_e$ distribution during the Late Pleistocene.

## RESULT

### Temporal fluctuation patterns of demographic history

The genomes of 527 species, including 238 mammals of 20 orders, 266 birds from 30 orders, 16 reptiles across 2 orders, and 7 amphibians within a single order, were used to reconstruct demographic fluctuations from 200 to 10 ka (Fig. 1A, table S1, and fig. S1). All species were extant, and the selection of species encompassed all zoogeographic regions (table S1 and fig. S2). The study encompassed 10.25% of species classified as "critically endangered" and "endangered" in the International Union for Conservation of Nature (IUCN) Red List (fig. S3).

Generalized additive models (GAMs) were used to simulate the temporal demographic histories of mammals [adjusted coefficient of determination ($R^2$) = 0.323, $P < 0.001$], birds (adjusted $R^2 = 0.158$, $P < 0.001$), reptiles (adjusted $R^2 = 0.385$, $P < 0.001$), and amphibians (adjusted $R^2 = 0.304$, $P < 0.001$). Our results indicated that, during the LGP, the demographic histories of mammals and reptiles showed a steady decline. In contrast, the demographic histories of birds and amphibians reached the lowest values around the Last Glacial Maximum (LGM; ~26 to 19 ka). In the Penultimate Glacial Period (PGP; ~194 to 135 ka), the demographic histories of mammals, reptiles, and amphibians steadily declined, while those of birds remained stable. Overall, compared to the PGP, during the LGP, the $N_e$ of each taxon was lower, and the demographic fluctuations are more intense (Wilcoxon rank sum test, $W = 30{,}332$, $P < 0.05$; Fig. 1B and fig. S4).

To investigate whether species with differing dispersal capacities exhibit distinct response patterns, we simulated temporal demographic

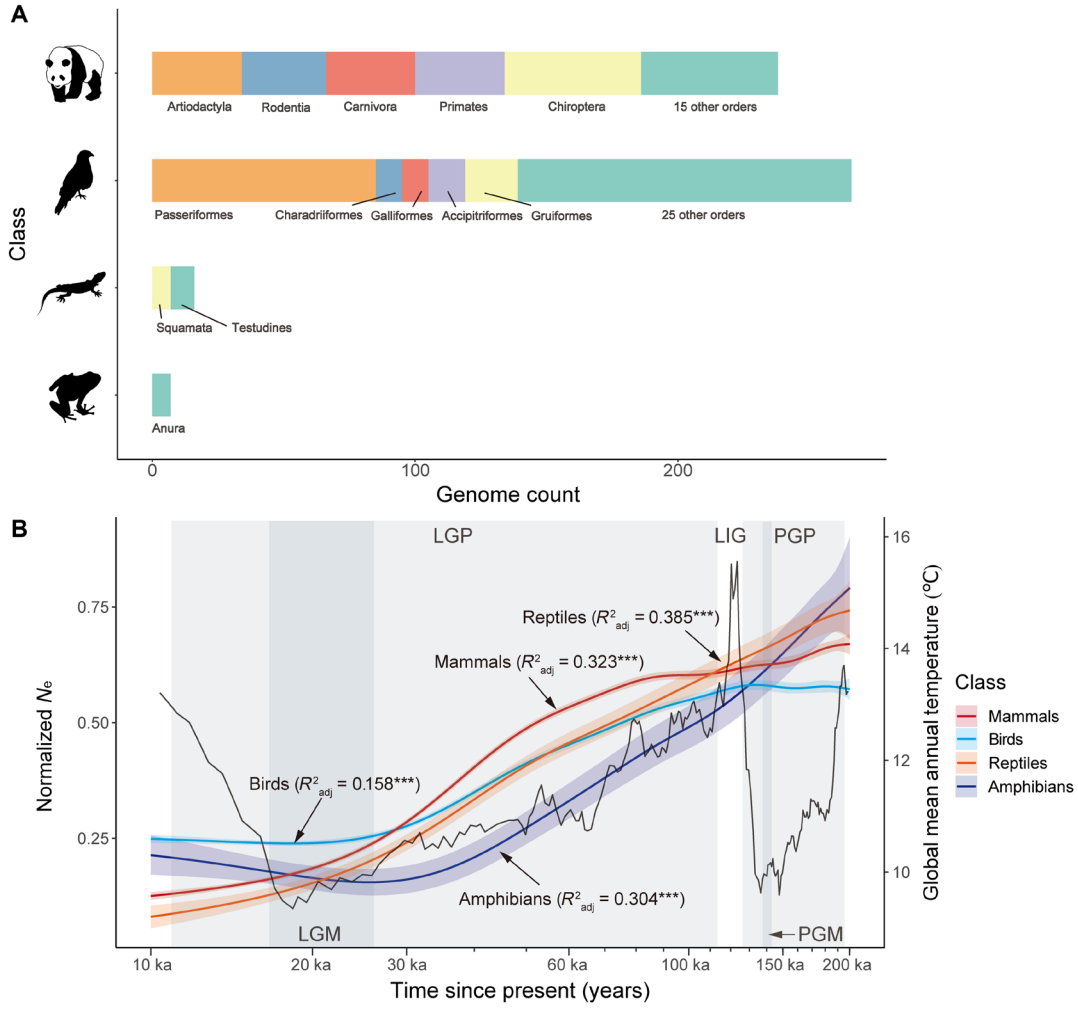


**Fig. 1. Genome data distribution across taxa and demographic histories of terrestrial vertebrates.** (**A**) Distribution of genomes across four taxonomic groups: mammals ($n = 238$), birds ($n = 266$), reptiles ($n = 16$), and amphibians ($n = 7$). (**B**) Demographic histories of different taxa. The black broken line represents the global mean annual surface temperature. $N_e$ of mammals and reptiles declined during the LGP (~115 to 11.7 ka), and $N_e$ of birds and amphibians reached its lowest values around the time of the Last Glacial Maximum (LGM; ~26 to 19 ka). During the Penultimate Glacial Period (PGP; ~194 to 135 ka), $N_e$ decreased steadily in mammals, reptiles and amphibians, while $N_e$ in birds remained stable.

fluctuations in the following: (i) bats (adjusted $R^2 = 0.257$, $P < 0.001$) and flying birds (adjusted $R^2 = 0.160$, $P < 0.001$); (ii) birds with diverse migration capabilities, including full migratory (adjusted $R^2 = 0.095$, $P < 0.001$), nonmigratory (adjusted $R^2 = 0.197$, $P < 0.001$), and flightless birds (adjusted $R^2 = 0.871$, $P < 0.001$). Comparing both, bats experienced a more severe decline from the Last Interglacial (LIG; ~130 to 115 ka) to the LGM than birds. Similarly, after the LGM, bat populations continued to decline. During the PGP, bats demonstrated a pattern of initial decline followed by a subsequent increase in response to temperature fluctuations (fig. S5). In addition, comparative analyses of birds with varying migratory capabilities revealed that flightless bird populations declined during both glacial periods. For migratory and nonmigratory birds, the population dynamics remained relatively stable during the PGP, declined from the LIG to the LGM, and increased after the LGM. Notably, birds with greater migratory abilities showed less pronounced fluctuations during glacial periods (fig. S6).

### Classification of interspecific demographic history fluctuations

Moreover, to illustrate the temporal fluctuation patterns of all studied species in the LGP, temporal $N_e$ patterns were further divided into 13 demographic clusters (Fig. 2 and fig. S7). Specifically, clusters 1, 3, and 12 comprised species whose demographic peaks during the Pleistocene-Holocene boundary (PHB; ~11.5 to 9.5 ka). Clusters 2 and 6 included species with demographic peaks in the Marine Isotope Stage 3 (MIS3; ~57 to 29 ka), MIS4 (~71 to 57 ka), and MIS5 (~130 to 80 ka). Clusters 4, 7, and 10 comprised species whose demographic peaks occurred during MIS4 and MIS5. Clusters 9 and 11 involved species with demographic peaks at both the PHB and MIS5. No discernible pattern was observed in clusters 5, 8, or 13 (Fig. 2). Additionally, no significant correlation was observed between the four taxonomic groups and demographic patterns ($\chi^2 = 45.219$, df = 36, $P = 0.140$). Mammals and birds were distributed among all demographic clusters; reptiles were distributed in clusters 2, 4 to 7, 10, and 12, while amphibians were distributed in clusters 1 to 4, 7, and 10 (fig. S8). Furthermore, the species IUCN statuses were uniformly distributed among the 13 demographic patterns ($\chi^2 = 60.804$, df = 60, $P = 0.447$).

### Spatiotemporal patterns of species richness and demographic history

To obtain spatial $N_e$ distributions for terrestrial vertebrates, species distribution models (SDMs) were used to project the suitable habitat of all studied species from 10 to 120 ka, at 10,000-year intervals. Considering the lack of population-level samples for most species, a single genome sample was adopted as a surrogate for population-level samples. The feasibility of this strategy was validated by comparing single sample and population-wide temporal and spatial $N_e$ values using 195 resequencing data of 22 geographic information-complete species (fig. S9 and table S2). On the basis of our findings, the intraspecific temporal $N_e$ patterns were much more similar than interspecific ones (Wilcoxon rank sum test, $W = 15{,}111{,}017$, $P < 0.05$; fig. S10). Spatially, the global $N_e$ distribution from single samples showed a strong correlation with that from population-level samples ($R^2 = 0.52$, $P < 0.05$; fig. S11). These findings suggest that, in the context of our study, $N_e$ data from a single sample can be approximated to substitute $N_e$ data at the population level.

Next, we compared the spatiotemporal $N_e$ patterns of 11 zoogeographic regions, including the Palearctic, Nearctic, Sino-Japanese, Saharo-Arabian, Afrotropical, Neotropical, Oriental, Madagascan, Australia, Panamanian, and Oceanian (Fig. 3A). Before the LGM, the global $N_e$ across all zoogeographic regions exhibited a downward trend. Thereafter, $N_e$ increased in all regions except for Afrotropical, Madagascan, Neotropical, and Oceanian regions (Fig. 3B and fig. S12). The global $N_e$ map for all taxa revealed the absence of the latitudinal gradient when $N_e$ was averaged across cells within 10° latitudinal bands (figs. S13 and S14). The species richness of the 527 terrestrial vertebrates remained stable over time (Fig. 3C and fig. S15). Our analysis revealed a weak linear relationship between $N_e$ and species richness across all time periods (fig. S16). The detailed spatiotemporal patterns of $N_e$ and species richness for mammals and birds are presented in figs. S17 to S24.

### Spatiotemporal patterns of $N_e$ hotspots

Due to global hotspot shifts affected by the numbers of taxa sampled for each area, to eliminate the interference of species richness on $N_e$ and clarify the spatiotemporal dynamics of $N_e$ hotspots, the standardized effect size of $N_e$ (SES-$N_e$) was calculated using a random shuffling algorithm with 1000 iterations, aiming to ensure more accurate quantification of the significance of $N_e$ hotspots (SES-$N_e \geq 1.96$ at an α level of 0.05 and in the top 5%). Subsequently, we constructed a spatiotemporal map to visualize the variability of these $N_e$ hotspots across geographic regions and over time (Fig. 4). $N_e$ hotspots shifted from Neotropical (120 to ~70 ka) to Afrotropical (60 to ~30 ka) and lastly to Palearctic (10 ka; Fig. 4 and fig. S25). Some $N_e$ hotspots, like Brazil's Cerrado (120 ka), the Horn of Africa and Central Chile (30 ka), and the southern cone of Neotropical (20 ka), correspond to the now recognized global biodiversity hotspots. Other hotspots, including the Andes (60 ka), the Bering Land Bridge (60 to 10 ka), the southern European peninsulas, and the Appalachian Mountains (20 ka), aligned well with the glacial refugia (Fig. 4). More details on spatiotemporal patterns and hotspots of demographic fluctuations for mammals and birds are shown in figs. S26 and S27.

### Factors affecting spatiotemporal patterns in the demographic history

We used spatial mixed-effects models (spaMMs) to investigate the potential effects of abiotic (mean annual temperature, mean annual precipitation, and elevation) and biotic factors (human disturbance) on the spatiotemporal patterns of the demographic history. Based on our results, the impacts of temperature, precipitation, elevation, and human disturbance varied across zoogeographic realms (Fig. 5). In middle- and high-latitude regions (Palearctic, Nearctic, Sino-Japanese, and Saharo-Arabian), the temperature had a positive effect on SES-$N_e$ from 120 to 50 ka but a negative effect from 40 to 10 ka. In low-latitude regions, especially in Neotropical, Australia, and Panamanian regions, there was a positive effect of temperature on SES-$N_e$ during the LGP (table S3). Regarding precipitation, there was a positive correlation between precipitation and SES-$N_e$ in Saharo-Arabian, Madagascan, and Afrotropical regions from 120 to 70 ka, whereas, in the Sino-Japanese, Neotropical, and Australia, precipitation was negatively correlated with SES-$N_e$. Regarding elevation, the effects were weak or nonsignificant in most zoogeographic regions. However, in the Neotropical region, SES-$N_e$ was positively correlated with elevation from 50 to 10 ka, while, in Afrotropical and Oceanian regions, the effects were negative from 90 to 50 ka. In addition, our research showed that human disturbance had significant negative impacts on SES-$N_e$ in the Palearctic, Australian, and Oceanian areas at the PHB (Fig. 5).

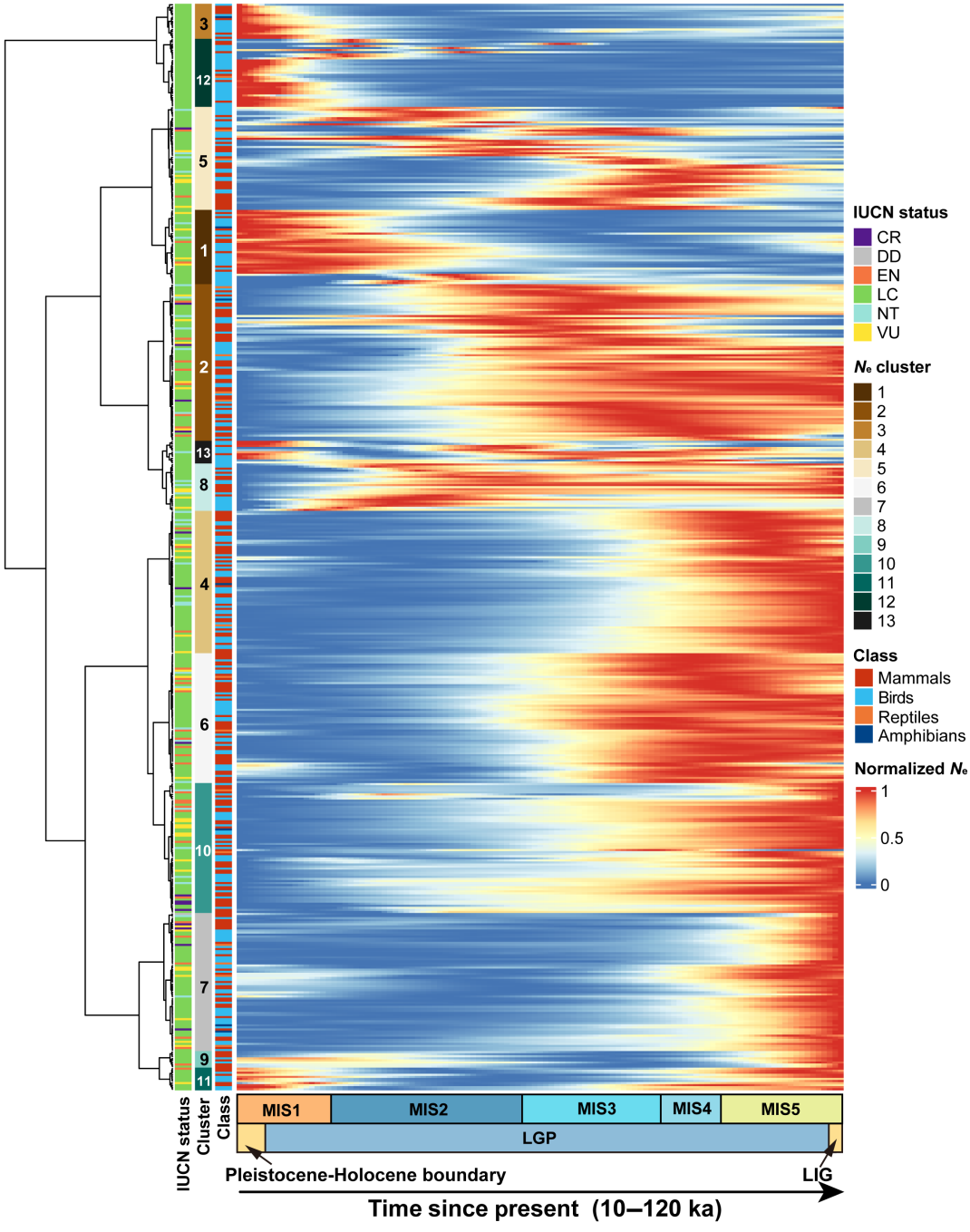


**Fig. 2. Clusters of temporal patterns of demographic fluctuations.** The heatmap illustrates the temporal fluctuations in population dynamics during the Late Pleistocene for 527 species, with each column showing the normalized $N_e$ over time for individual species. The chromatic scale indicates normalized $N_e$ values, with hues approaching red signifying higher $N_e$ and those nearing blue indicating lower $N_e$. Adjacent to the heatmap, the legends identify the taxonomic class, IUCN conservation status, and the cluster affiliation of each species. Below the heatmap is the geological history period corresponding to the $N_e$ fluctuations. On the basis of the fluctuation patterns of normalized $N_e$, the demographic histories were classified into 13 clusters.

## DISCUSSION

This study presents, to our knowledge, the first global assessment of the demographic histories of terrestrial vertebrates during the Late Pleistocene. According to our study results, the $N_e$ of all four taxonomic groups declined from the LIG to the LGM. After the LGM, the $N_e$ of birds and amphibians slightly increased, whereas that of mammals and reptiles continued to decline (Fig. 1B). The contrasting $N_e$ trajectories among vertebrates suggest that glacial period dynamics were predominantly shaped by the differential strengths of environmental filtering and dispersal, two of the four fundamental processes in macroscale community ecology (selection, ecological drift, dispersal, and speciation) described by Vellend (*21*). For mammals, the

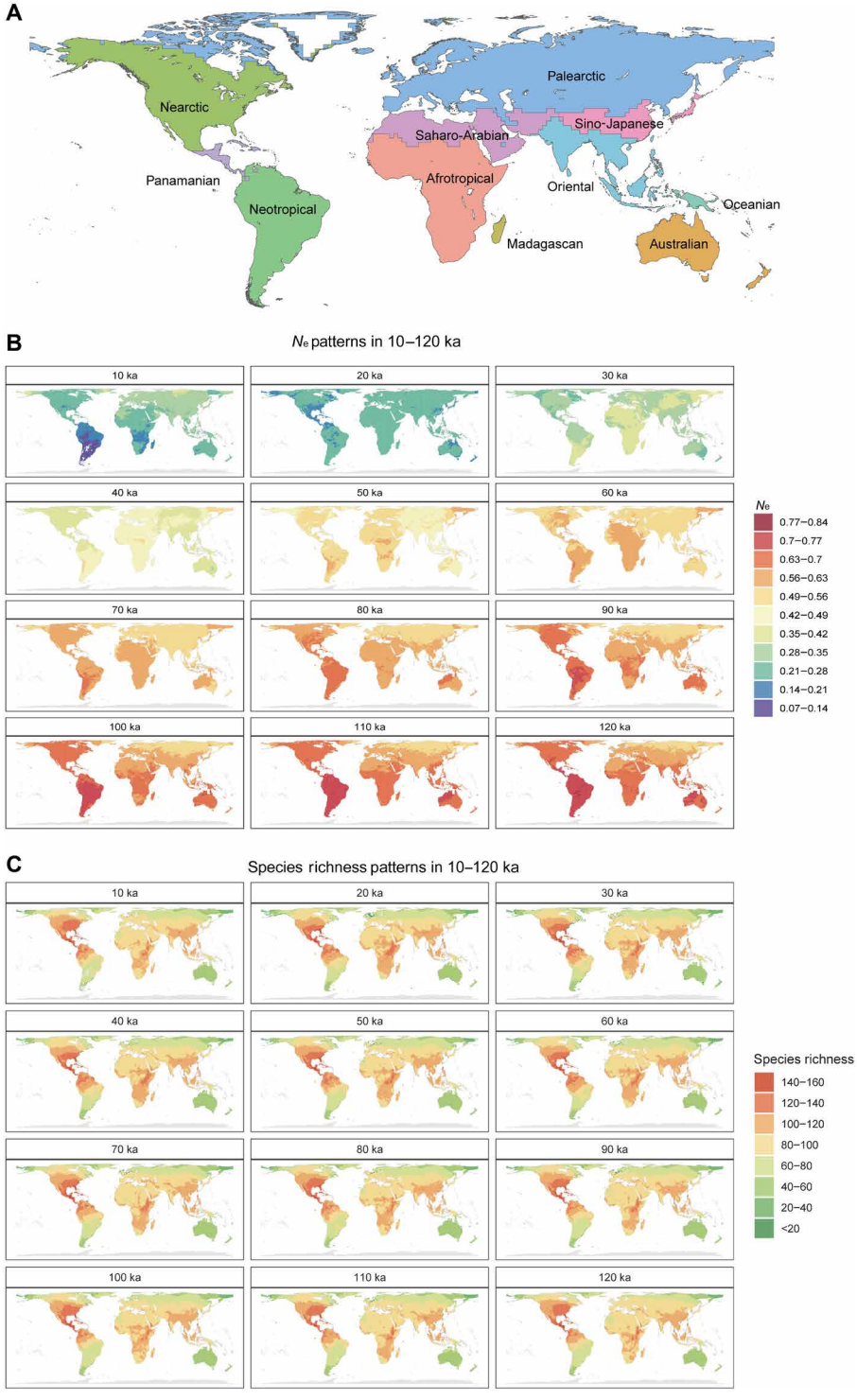


**Fig. 3. Spatiotemporal dynamic patterns of $N_e$ and species richness during the Late Pleistocene.** (**A**) Wallace's zoogeographic regions of the world (*85*). (**B**) Spatial variation in the normalized $N_e$ of terrestrial vertebrates during the Late Pleistocene. The color gradient indicates the relative variation of $N_e$: Deeper red indicates higher $N_e$, while deeper blue represents lower $N_e$. (**C**) Species richness patterns for terrestrial vertebrates during the Late Pleistocene. The gradient from deep red to deep green shows a shift from higher to lower species richness, respectively.

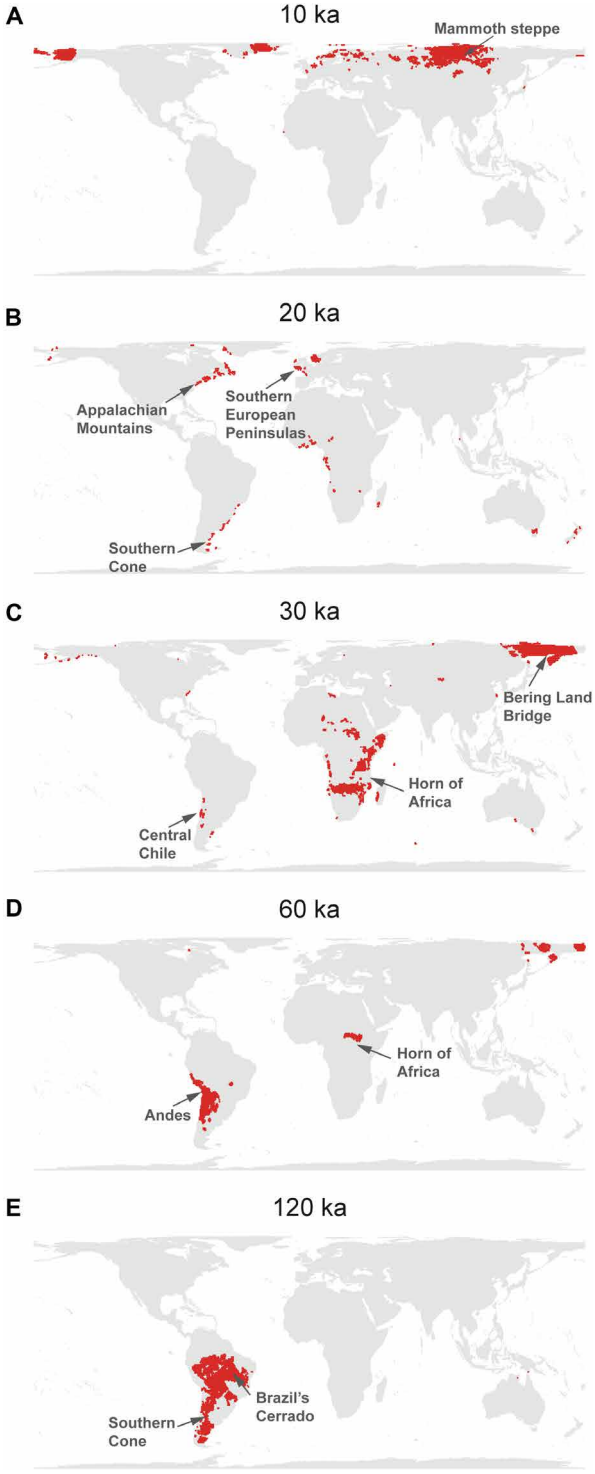


**Fig. 4. Global $N_e$ hotspots shift pattern (10 to 120 ka).** (**A** to **E**) The temporal shift in the standardized effect size of $N_e$ (SES-$N_e$) across all grid cells for different time periods: (A) 10 ka, (B) 20 ka, (C) 30 ka, (D) 60 ka, and (E) 120 ka. Red areas indicate regions where the SES-$N_e \geq 1.96$ ($\alpha = 0.05$), corresponding to the top 5% of the SES-$N_e$ values. The names of the vital geographic areas have been labeled on the map.

continued $N_e$ decline aligned with paleontological evidence of megafaunal extinctions (*22*, *23*), likely driven by intensified selection pressures arising from synergistic climatic stressors and human disturbances (*24*). Compared with the findings in mammals, birds displayed greater demographic resilience during the glacial period. Moreover, environmental filtering is potentially more important in mammals than in birds. Additionally, bird populations with higher dispersal capacity exhibited enhanced resilience to glacial cycles (fig. S6). These patterns were consistent with Vellend's theoretical framework positing that dispersal mediates directional selection dynamics by decoupling populations from local environmental filters. Superior dispersal capabilities enabled birds to track shifting habitats more effectively, enhancing their survival and competitive advantage in harsh glacial environments and thereby increasing their fitness (*25*). For reptiles, in which temperature determines offspring sex (*26*), a cold climate might lead to population bias in sex ratios, potentially imposing an environmental filter that reduced the overall population size (*27*). For amphibians, the drought caused by the ice age might have limited habitat availability, contributing to the decrease in $N_e$ (*28*). When the glaciers melted after the LGM, amphibians had more available flowing water and greater opportunities for reproduction, and the relaxation of the effects of environmental filtering on amphibians led to a rebound in $N_e$.

Additionally, we simulated demographic histories during the PGP as a second "natural experiment." Notably, bird populations remained stable during this period, although the populations of other taxa declined, the size of these decreases was much smaller than that observed during the LGP (Fig. 1B). We attributed this finding to the impact of climatic oscillations during glacial periods. The LGP was characterized by centennial- to millennial-scale climate oscillations, termed Dansgaard-Oeschger (D-O) cycles. Compared with the findings during the cooling period of the LGP (MIS2 to MIS4), the pacing of D-O cycles was almost twofold longer during the cooling period of the PGP (MIS6; ~191 to 130 ka) (*29*). The more rapid climate changes of the LGP caused more intense responses of species to glacial periods (*30*). Consistent with Vellend's theory, this finding denoted climate oscillation frequency as a critical factor for environmental selection intensity. The rapid LGP climate shifts exceeded the adaptive capacities of most species, thereby intensifying environmental selection-driven population decline. Notably, our study bridges genomic-level analyses with macroscale community ecology, providing reciprocal validation and insights into the underlying mechanisms shaping demographic fluctuations.

Temporally, the $N_e$ patterns for all studied species were divided into 13 demographic clusters (Fig. 2A). This result is inconsistent with that of Germain *et al.* (*4*), who segmented the demographic history of birds into seven clusters. This discrepancy may be attributed to differences in time periods and taxonomic scope. Our research comprised 527 species of terrestrial vertebrates, was not limited to birds alone, and focused on the Late Pleistocene, whereas their study spanned from 1 million years to 30 ka. We found that the $N_e$ trend increased in some species during periods of climate cooling (Fig. 2A). These observations suggest that not all species will be negatively affected by temperature decreases. Functional traits, such as dispersal ability or life-history characteristics, may affect the demographic response of each species to climate change (*31*, *32*). For

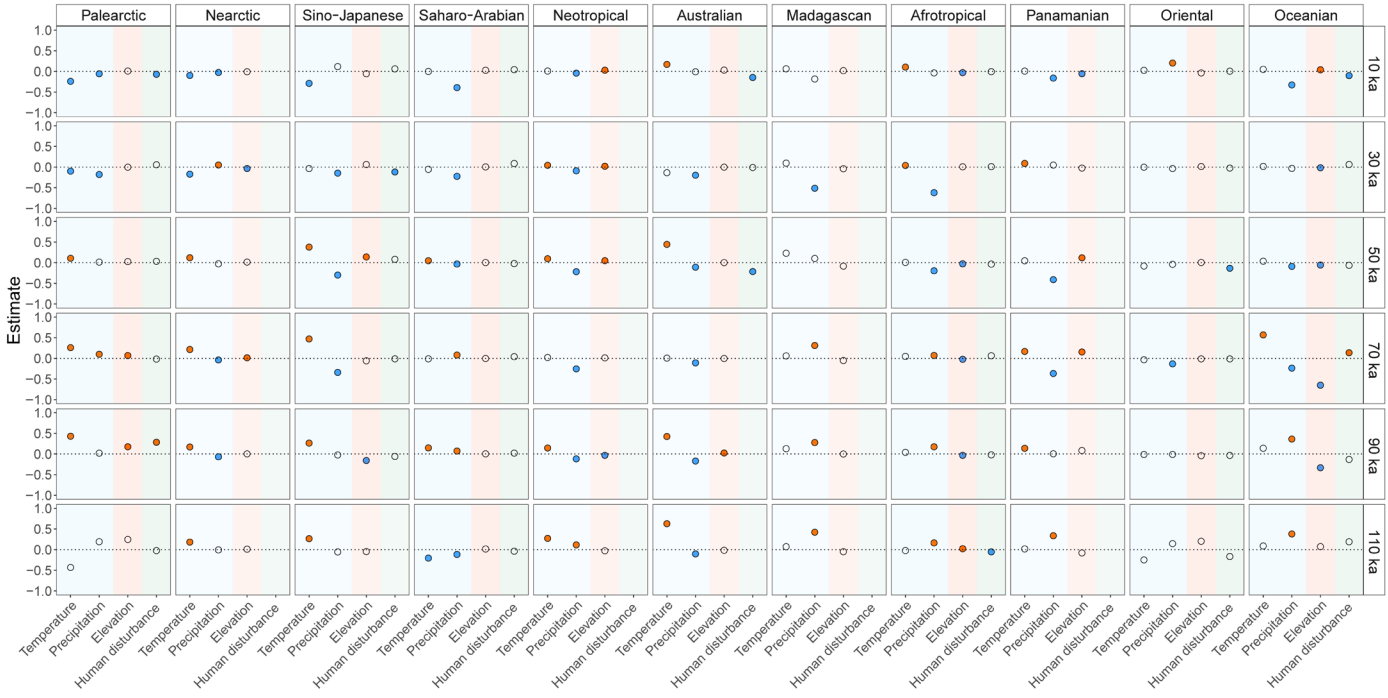


**Fig. 5. Determinants of the global SES-$N_e$ patterns in 11 zoogeographic realms.** Standardized coefficients, estimated using spaMM models, illustrate the relative effects of temperature, precipitation, elevation, and human impacts on the SES-$N_e$ of 527 terrestrial vertebrates during the Late Pleistocene. Red points suggest significantly positive coefficients, blue points indicate significantly negative coefficients, and gray points denote nonsignificant effects.

instance, birds with larger body mass, lower hand-wing index, and smaller egg mass are more likely to have lower $N_e$ under cooling conditions (*4*). In addition, the demographic history bottlenecks of certain mammals are associated with breeding habitat and mating system variation (*31*). Furthermore, changes in competitor abundances (i.e., compensatory dynamics) provide opportunities for population expansion. Collectively, these patterns underscore the varied demographic responses of species with different traits and across taxa to climate change.

The $N_e$ level determines a population's ability to adapt to environmental change and is a notable factor for the extinction risk (*33*). Consequently, examining $N_e$ hotspots can reveal drivers for population growth and improvements in species viability within these regions. This study introduced the SES-$N_e$ concept to quantify spatial $N_e$ hotspots for 527 terrestrial vertebrate species, mitigating the effects of species richness and allowing for more accurate, standardized comparisons of $N_e$ across regions, thereby supporting global biodiversity conservation. Spatiotemporally, the global SES-$N_e$ patterns during the Late Pleistocene revealed some SES-$N_e$ hotspots aligning with globally recognized biodiversity hotspots and refugia. Historical population changes considerably influence current biodiversity hotspots. During the LIG, SES-$N_e$ hotspots were consistent with many contemporary biodiversity hotspots (*34*), such as South America, particularly Brazil's Cerrado (Fig. 4E). Brazil's Cerrado region is covered with tropical savannas and is one of the most important water sources in South America. Plants in this area store a large amount of underground water to survive extreme climatic conditions, providing a food source for animals (*35*). Our research revealed, under harsh conditions, certain regions of SES-$N_e$ hotspots aligned with areas historically recognized as refugia during the LGP (Fig. 4). For example, during the LGM, the southern European peninsulas (Iberian and Balkan) emerged as SES-$N_e$ hotspots (Fig. 4B), serving as refugia for numerous plant and animal species across Europe during the Pleistocene ice ages (*36*). Similarly, the Andes were identified as a SES-$N_e$ hotspot from 120 to 60 ka, being regarded as refugia (Fig. 4D). This is because west of the Andes remained ice free during peak glaciation periods, with a consistently humid climate, providing suitable habitats for numerous species. The Appalachian Mountains also functioned as a glacial refuge during the LGM (Fig. 4B). In addition, the northeast of Siberia and the northwest of the Nearctic became SES-$N_e$ hotspots at 10 ka (Fig. 4A). In these regions, the ice sheet expansion probably provided numerous available habitats for high-latitude distribution species. During this period, northern Siberia, Alaska, and the Yukon became refugia for megafauna in the mammoth steppe (*37*, *38*). Our results suggest that genomic approaches could help identifying biodiversity hotspots and refugia across ancient periods.

In this study, we found that climate change had a substantial long-term impact on the demographic histories of terrestrial vertebrates during the Late Pleistocene, while human disturbance did not have substantial impact until 10 ka. During the cooling period, the SES-$N_e$ exhibited a positive correlation with temperature in the Neotropical, Australia, and Panamanian regions (Fig. 5). These low-latitude areas have stable climates and serve as climatic refuges for species with low vagility and small geographical ranges (*39*). As the sea level fell during the LGP, the continental shelf was exposed, providing a wider distribution area for species (*40*). However, our research exhibited a negative spatial correlation between SES-$N_e$ and temperature in middle and high latitudes from 40 to 10 ka (Fig. 5). This may be because cold environments enable species to develop

evolutionary adaptations. Throughout the glacial-interglacial cycles, an extended period of climatic fluctuations, the equatorial region consistently maintained a warm climate (at 30° to 40°C between the Paleocene and Pliocene). In contrast, higher latitudes were exposed to marked climatic variation (0° to −80°C). Therefore, species living in cold environments exhibited greater cold tolerance than those in warmer environments (*41*).

Regarding human disturbance, current views argue that population declines in extant megafauna were associated with human expansion rather than climate change during the Late Pleistocene and Early Holocene. Further, our study showed that the influence of human disturbance on the demographic fluctuations of terrestrial vertebrates varied geographically. The $N_e$ exhibited a negative correlation with human disturbance in the Palearctic, Australian, and Oceanian regions at the PHB (10 ka; Fig. 5). The most prominent example of human disturbance in the Palearctic is the woolly mammoth (*Mammuthus primigenius*). $N_e$ in woolly mammoths remained comparatively stable throughout the climatic oscillations of the entire Late Pleistocene, but there was a marked reduction in population and heterozygosity at the PHB (*42*, *43*). During the same period, the woolly mammoth disappeared from most parts of the Palearctic, with only small, isolated populations surviving on islands off the coast of Siberia and Alaska up to the Holocene (*44*). In Eurasia, the pulsed demise of megafauna coincided with the initial spread and subsequent population growth of modern humans (*22*). Further, we speculate that the disappearance of $N_e$ hotspots in the Iberia Peninsula may be associated with human disturbance. Another possibility is that a mismatch between the human niche and Palearctic cold-adapted species causes a negative correlation between $N_e$ and human disturbance. In Australia, humans were present in Australia already at 48 ka (*45*). During the Late Pleistocene, ~55 mammalian species were lost from Australia (*46*). Many specific species in Australia could not evolve traits to adapt to human overkill, resulting in population decline and even extinction (*22*). In general, the past baseline of the impact of climate change and human disturbance on biodiversity is the foundation for conservation decisions and future planning, and this is exactly what this study provides.

Additionally, using pairwise sequential Markovian coalescent (PSMC) to reconstruct population fluctuation highlights the critical role of population genomics in studying species' long-term dynamics, with implications for informing conservation and restoration efforts (*47*). However, using demographic histories from a single individual as surrogate for population history represents a limitation of our study. Despite the recent increase in population genomics studies, there is a lack of datasets providing detailed geographic coordinates linked to sample identifiers. This prevented conducting more precise spatial analyses at the population level. Moreover, most species included in this study are not endangered, endangered species comprising only 10.25% of the total. Given that endangered species may be more vulnerable to the impacts of climate change and human disturbance (*48*), our results may underestimate the effects of human interference on vertebrates during the Late Pleistocene. However, a global analysis of endangered species was not feasible due to limitations in genomic data. An expanding repository of genetic data will allow elucidating the spatiotemporal $N_e$ patterns at the population level and investigating the impacts of climate change and human disturbance on endangered species during the Late Pleistocene. Furthermore, the PSMC method inferred historical population dynamics under the assumption of panmictic populations, neglecting the spatial genetic structure (*49*). However, the population structure or changes in gene flow between populations can bias the PSMC estimates of $N_e$ (*50*–*52*). Given the absence of a priori information on population connectivity dynamics during the Late Pleistocene for the investigated species, obtaining detailed information on their population structures is challenging. We assumed that the observed population trajectories reflect both historical demographic processes and population structure, following Germain *et al.* (*4*). Notably, PSMC's assumption of neutral evolution neglected pervasive background selection, a linked selection process that reduces genetic diversity near deleterious mutations as they are purged (*53*). This oversight could have influenced the reconstruction of demographic history. Future research could use a structured coalescent model to better disentangle these effects (*54*). Although not entirely precise, our current comparative framework represents a pragmatic compromise solution that balances complexity and feasibility, providing a conservative yet practical approximation of historical demographic trends.

In conclusion, our study provides evidence supporting the hypothesis that climate and human disturbance caused the vertebrate population contraction during the Late Pleistocene. Specifically, climate exerts a persistent influence on $N_e$, while human disturbance primarily affects specific zoogeographic regions at the PHB. Moreover, our innovative approach to quantify $N_e$ spatiotemporal patterns revealed that the SES-$N_e$ hotspots vary over time in response to climate. Despite the inconsistent spatiotemporal dynamics of $N_e$ and species richness, they closely align with established biodiversity hotspots and ice age refuges. Furthermore, reconstructing demographic histories offers an innovative approach to evaluate species vulnerability to climate change. Our analysis of global vertebrate population dynamics in the Late Pleistocene provides a distinctive perspective on species conservation across various zoogeographic realms and taxa in future climate change scenarios.

## MATERIALS AND METHODS

### Vertebrate genomes and metadata

In this study, reference genome assembly and short-read data accessions were obtained from the National Center for Biotechnology Information (NCBI; www.ncbi.nlm.nih.gov/). The keywords "Mammalia," "Aves," "Lepidosauria," and "Amphibia" were used to collect published terrestrial vertebrate genome information by March 2022. Then, genomes with Sequence Read Archive (SRA) information were screened, and those of domestic species were removed. For species with multiple genomes, two standards were applied in selection. First, NCBI reference sequence and genomes with longer contig N50 were preferentially chosen. In this step, 907 species, including 384 mammals, 445 birds, 52 reptiles, and 26 amphibians were included (table S4). Second, species were persistently selected from the aforementioned dataset when fulfilling the criteria for demographic reconstruction (as mentioned below) and having geographical data. Last, 527 species, comprising 238 mammals, 266 birds, 16 reptiles, and 7 amphibians, were used for further analyses (table S1).

### Generation time and mutation rate

For all species, we collected metadata on conservation status and generation time. Generation time data of each species were obtained from published literature and databases (table S5). The phylogenetic relationships were reconstructed on the basis of fourfold degenerate sites [four-dimensional (4D) sites] of single-copy orthologous genes

to estimate the divergence time ($t$). To this end, we used miniprot version 0.2-r120-dirty with default parameters to predict orthologous genes for each species, using the human orthologous protein sequence as reference (*55*). Two selection criteria were applied to the initial set of 8023 orthologous genes: (i) The orthologous genes of each gene had to exhibit a sequence similarity of ≥40% to their human counterparts, and (ii) the aggregate mean and median sequence similarities for each gene should be >70%. Subsequently, 2461 genes were selected for subsequent analyses. To infer the phylogenetic relationships, all coding sequences were aligned according to their codons using the Muscle v3.8.31 algorithm (*56*) with default parameters and pal2nal (v.14) software. Next, we concatenated all alignments and trimmed them using trimAl version 1.4 (*57*). Thereafter, 4D sites were meticulously extracted from the curated alignments. Using these data, a robust super matrix comprising 12,027 base pairs was constructed, representing a diverse taxonomic set of species. Last, phylogenetic inference was performed with RAxML version 8.2.12, using the GTRGAMMAI model of nucleotide substitution with 1000 bootstrap replicates, to ascertain the reliability of the inferred phylogeny (*58*). Divergence times ($t$) were estimated by r8s based on 32 fossil records from published literature (fig. S28 and table S6) (*59*). Furthermore, to quantify pairwise genomic differences ($D$) between species, the genome of their closely phylogenetic relative species was used as reference to generate pairwise whole-genome alignments using LAST (version 802) (*60*). The "lastal" command with the parameter -E 0.05 was used to align the reference for each genome. Then, best pairwise aligned blocks were obtained using the "maf-swap" command to change the sequence order. Last, MULTIZ (version 11.2) (*61*) was used to merge pairwise alignments and obtain the number of different bases.

The species-specific mutation rate (μ) was scaled as

$$\mu = \frac{D}{2t} \times g$$

where $g$ is the generation time for each species, $D$ is the observed frequency of pairwise differences between the two species, and $t$ is the divergence time of the two species.

### Vertebrate distribution and climatic data

The present geographical coordinates for each species in the four vertebrate groups were acquired from the following databases: (i) Global Biodiversity Information Facility (GBIF; https://doi.org/10.15468/dl.495qsy, https://doi.org/10.15468/dl.wmbbk6, https://doi.org/10.15468/dl.xz8gr4, and https://doi.org/10.15468/dl.nmnmd9 for reptiles, amphibians, mammals, and birds, separately; accessed 11 July 2022), (ii) Vertebrate Natural History Collections Network (www.vertnet.org/), (iii) iNaturalist (www.inaturalist.org/), (iv) iDigBio (www.idigbio.org/), (v) Projecting Responses of Ecological Diversity In Changing Terrestrial Systems (www.nhm.ac.uk/our-science/our-work/biodiversity/predicts.html), (vi) The Atlas of Living Australia (www.ala.org.au/), and (vii) the National Animal Collection Resource Center (http://museum.ioz.ac.cn/index.html). Moreover, we compiled geographical range maps for the four vertebrate groups sourced from the IUCN Red List (www.iucnredlist.org/) and BirdLife database (www.birdlife.org/). Subsequently, we eliminated all GPS coordinates beyond the confines of the polygons delineated by the IUCN and BirdLife.

As georeferencing errors, inaccuracies, and biases are prevalent in occurrence databases, it is imperative to implement a rigorous filtering protocol to ensure dataset integrity. In this study, the R package CoordinateCleaner (*62*) was used to meticulously filter out coordinates that (i) featured latitude or longitude coordinates out of their ranges [(−90, 90) and (−180, 180), respectively]; (ii) were identified as outlier coordinates; (iii) had both coordinates set to zero or coordinates equal to each other (i.e., latitude equals longitude); or (iv) were assigned to country or province centroid, the open ocean, the GBIF headquarters, urban areas, or the location of biodiversity institutions (museums, zoos, botanical gardens, and universities). To mitigate spatial autocorrelation and prevent information redundancy, we only maintained one record per grid cell for each species. Species with <6 presence points were excluded.

Current and the Late Pleistocene bioclimatic variables were extracted from a high-resolution terrestrial bioclimatic (*63*). For the Late Pleistocene bioclimatic variables, 19 bioclimatic variables layers were obtained at 12 time periods (10,000 years intervals from 10 to 120 ka) at 0.5° resolution. Thereafter, we calculated Pearson's correlation coefficients ($r$) among the variables and only one variable with more ecological meaning was retained if two were highly correlated ($r > 0.8$). Last, the following six bioclimatic variables layers were maintained for each time period: BIO1 (annual mean temperature), BIO10 (mean temperature of warmest quarter), BIO12 (annual precipitation), BIO13 (precipitation of wettest month), BIO14 (precipitation of driest month), and BIO17 (precipitation of driest quarter).

### Demographic reconstruction

To reconstruct the demographic history of each taxonomic group, fastp (*64*) was first used to filter low-quality reads in the raw SRA data of each species using default parameters. Moreover, the remaining high-quality reads were aligned to the genome of the corresponding species using BWA software (version 0.7.17) (*65*); polymerase chain reaction duplicates were removed using "MarkDuplicates" in Picard (version 2.21.6) (http://broadinstitute.github.io/picard). To obtain high-quality single-nucleotide polymorphisms (SNPs), we applied the following filtering criteria: (i) removing homozygous SNPs and SNPs with >2 alternative alleles, (ii) eliminating SNPs with a read depth of $<^1/_3$ or >2× the average read depth across the genome, and (iii) removing SNPs with root-mean-square mapping quality of <50.

The PSMC method was applied for reconstructing $N_e$ for each species during the Late Pleistocene (*6*). Species whose heterozygosity mapping data coverage <18×, or those with >25% missing data, were excluded from the analysis (table S7) (*4*). Furthermore, we evaluated the impact of different parameters on the multispecies PSMC estimation, including the number of free atomic time intervals (-p option; fig. S29), upper time limit to most recent common ancestor (-t option; fig. S30), and initial $r = \theta/\rho$ value (-r option; fig. S31). The final parameter determined was "-N30 -t5 -r5 -p 4 + 251*1 + 4 + 6 + 10." Afterward, the -R command in "psmc_plot.pl" was used to keep the temporary files to obtain the $N_e$ estimates (table S8).

### Species distribution models

To simulate suitable habitats for each species, we generated a buffer area surrounding the presence records for each species. The buffers' radii varied among taxonomic groups because of their different migration abilities (amphibians, 2000 km; reptiles, 3000 km; mammals, 3000 km; and birds, 4000 km) (*66*). Thus, 10,000 pseudoabsence records were randomly sampled within the buffer area range to prevent overprediction (*67*).

For each species, generalized linear model, GAM, random forest, and maximum entropy model were used to simulate species

distribution using the R package biomod2 (*68*). Moreover, model performance was assessed by the true skill statistic (TSS) (*69*), with 70% of data points used for training and the other 30% for testing for each replication. Each algorithm was repeated four times, providing a fourfold internal cross-validation. A threshold of TSS > 0.5 was applied to select each model (*66*). Models that did not reach this threshold were subsequently removed from the final ensemble model (*66*, *69*). Last, the TSS values of all species ensemble models were > 0.59, and the average TSS was 0.82 (fig. S32).

The above modeling strategy was used to project the potential distribution of each species. These projections were performed under current and the Late Pleistocene (from 120 to 10 ka in 10-ka intervals) climatic conditions. Later, a buffer was used as the maximal dispersal distance to exclude the suitable habitats outside each buffer. At last, for all species, their suitable habitats were converted to binary maps based on species-specific max TSS thresholds for each time period (*68*).

### Simulation of demographic patterns and robustness test

To investigate the demographic fluctuation patterns during the LGP and PGP, GAM (*70*) was used to simulate the $N_e$ trend across the four taxa. A time span from 10 to 200 ka was subjected to a logarithmic transformation and subsequently divided into 190 equally sized time periods for each species. We chose the $N_e$ values of the corresponding time and used a min-max normalization to rescale values between 0 and 1. To quantify the demographic fluctuation intensity of each class during the temperature rise and fall phases of LGP and PGP, we calculated the derivatives of the fitted curves for each time point in the four taxa using the "derivatives" function in the R package gratia (*71*). Subsequently, we divided the entire period into four distinct intervals and applied the Wilcoxon test to compare derivatives among the four taxa across these intervals: (i) before the PGM (~140 ka), when global temperatures exhibited a declining trend (200 to 140 ka); (ii) from the PGM to the LIG (140 to 120 ka), characterized by an increasing trend in global temperatures; (iii) from the LIG to the LGM (120 to 19 ka), marked by a decline in global temperatures; and (iv) after the LGM (19 to 10 ka), when global temperatures exhibited an increasing trend.

To investigate whether species with different dispersal capacities exhibit different response patterns, we compared the population fluctuation patterns between: (i) bats and flying birds and (ii) birds with different migration abilities. Specifically, we classified the birds in this study into three categories: fully migratory, nonmigratory, and flightless, based on Sayol *et al.* (*72*) and Sheard *et al.* (*73*). We excluded penguins and ostriches from the flightless category because their flight abilities and dispersal capacity were irrelevant. Then, we modeled the $N_e$ trend using GAMs, calculated the derivatives of the fitted curves, and subsequently applied the Wilcoxon test to compare the mentioned groups.

Because the PSMC outputs depended critically on the mutation rate and generation time (*6*), we evaluated the robustness of our demographic trend results by generating random input matrices across biologically plausible ranges of species-specific mutation rates and generation times. Based on empirical estimates of intraspecific variation in generation time metrics, we constrained the potential fluctuation range of generation times to $\pm^1/_3$ (*74*). The mutation rate variation ranges for vertebrates were defined on the basis of the 95% confidence intervals of mutation rate estimates reported by Bergeron *et al.* (*75*) (±12% for mammals, ±40% for birds, and ±54% for reptiles). For amphibians not included in the aforementioned study, we conservatively adopted the maximum observed variation range (±54%) across all analyzed taxa. Subsequently, for each species, we performed 100 independent random samplings of generation time and mutation rate within their respective defined ranges, producing 100 distinct PSMC temporal trajectories per species. Further, we executed a bootstrapping procedure in which a single trajectory was randomly subsampled from each species' ensemble, from which identical temporal intervals were extracted to model $N_e$ trajectories across all four taxonomic groups using GAMs. This process was iterated 100 times to ensure robustness in cross-species demographic comparisons. Last, we conducted secondary GAM fitting on the 100 simulated trajectories and performed the Wilcoxon tests comparing these simulations with the original demographic reconstruction presented in Fig. 1B. Statistical evaluation revealed no significant divergence between the two fitting outcomes (Wilcoxon's test; mammals: $W = 18{,}389$, $P = 0.89$; birds: $W = 17{,}313$, $P = 0.39$; reptiles: $W = 19{,}036$, $P = 0.46$; and amphibians: $W = 19{,}927$, $P = 0.12$; fig. S33), demonstrating that variations in the generation time and mutation rate parameters had only a minimal impact on our conclusions.

### Clustering analysis of demographic patterns and robustness test

To investigate the interspecific variability in demographic fluctuation patterns during the Late Pleistocene and assess their correlation with taxonomic classification and IUCN conservation status, a clustering analysis was applied on the basis of normalized $N_e$ values (*4*). We clustered the $N_e$ values of 527 species using time-series clustering, a clustering algorithm for handling dynamic data (*76*). Because we expected to cluster on the basis of the overall $N_e$ dynamic change, the dynamic time warping (DTW) distance was used as a dissimilarity measure. DTW is a shape-based time-series clustering method that aligns two time series to find their optimal match (*76*). Herein, the "tsclust" function in the R package dtwclust (*77*) was used to split the clustering dendrogram into $k = 2$ to 15 groups to find the most suitable number of clusters. The cluster evaluation metrics were standardized using six cluster validity indices: Silhouette, score function, Davies-Bouldin, modified Davies-Bouldin (DBstar), Dunn, and COP. In addition, we split the clustering dendrogram using the "cutree" function in the R package dendextend (*78*).

We also evaluated the sensitivity of our clustering outcomes to variations in the mutation rate and generation time. First, for each species, we quantified parameter-perturbed trajectory dissimilarity by calculating DTW distances between the $N_e$ trajectory used in our clustering analysis and 100 $N_e$ trajectories generated under random mutation rate and generation time perturbations. Second, we computed interspecies DTW distances under equivalent parameter variations, assessing the robustness of our clustering. Our comparative trajectory analysis revealed that the DTW distances between parameter-perturbed trajectories (mutation rate and generation time variations) were significantly smaller than those observed in interspecific comparisons (Wilcoxon's test, $W = 2.52 \times 10^9$, $P < 0.01$; fig. S34). This clear dissociation demonstrated that mutation rate and generation time parameters exerted minimal influence on the clustering result.

### Spatial patterns of $N_e$ and species richness during the Late Pleistocene

To map the global $N_e$ distribution during the Late Pleistocene, all SDM distribution maps were transformed into the Behrmann equal-area

projection grid. Thereafter, the average $N_e$ and the studied species richness were calculated for each grid cell. To determine the species richness, we calculated the total number of species within the grid cell (*79*). Thereafter, the $N_e$ values of each species within the grid cell were calculated from 120 to 10 ka. Then, the total number was divided by that of species surveyed in the grid cell. To gain a more intuitive understanding of $N_e$ changes over time in different zoogeographic realms, we used the GAM (*70*) to simulate the $N_e$ trend. In addition, the Spearman correlation between $N_e$ and species richness was tested with linear models. The effects of latitude on $N_e$ were investigated using linear models. To identify significant $N_e$ hotspots, we calculated the SES-$N_e$ based on the species presence/absence matrix and the normalized $N_e$ for each species from 120 to 10 ka. Specifically, for each grid cell, 1000 null distributions of expected mean $N_e$ values were generated by shuffling species labels, with a constant total number of grid cells occupied per species, using the "randomizeMatrix" function in the R package picante (*80*). Then, we calculated SES-$N_e$ value of each grid cell by dividing the difference between the simulated $N_e$ ($N_e$_simulated) and the expected mean $N_e$ ($\overline{N}_e$_randomized) values by the SD of the null distribution ($\sigma_{N_e\_randomized}$), mathematically defined as

$$\mathrm{SES}-N_e=\frac{N_e\_\mathrm{simulated}-\overline{N}_e\_\mathrm{randomized}}{\sigma_{N_e\_\mathrm{randomized}}}$$

This method allows comparing $N_e$ values across regions using consistent criteria, even despite significant differences in species richness, thereby eliminating the confounding effects of species richness (*81*). To avoid fragmentation, continuous grids with SES-$N_e$ values of $\geq$1.96 ($\alpha = 0.05$) and in the top 5% were identified as $N_e$ hotspots.

### Comparison of population and single species $N_e$

We used the PSMC of an individual to represent the demographic fluctuations of the entire population; therefore, we examined the diversity of PSMC patterns intra- and interpopulation. When interspecific variations outweighed the intraspecific variance, the individual PSMC served as proxy for the population-level PSMC, enabling cross-species demographic comparisons. Accordingly, we collected a total of 195 resequencing data of 22 species with detailed geographic information, including nine mammals with 83 SRA sequences and 13 birds with 112 SRA sequences (fig. S9 and table S2). In addition, we adopted the PSMC approach to reconstruct the population history of the 195 SRA samples, as indicated in the "Demographic reconstruction" section. Subsequently, the DTW distance (explained in the "Clustering analysis of demographic patterns and robustness test" section) of $N_e$ over the time curves for each species was calculated by comparing each sample pair. In addition, we calculated the DTW distances for $N_e$ curves across species. Then, we applied the Wilcoxon test to compare DTW differences between intraspecific and interspecific populations. To assess whether the $N_e$ of a single sample can suffice as a proxy for population-level samples in spatial analysis, intraspecific mean and individual sample $N_e$ were spatially mapped, and the correlation between these two sets of results was compared with that of the linear model.

### Spatial regression analysis of $N_e$ and environmental factors

To identify the factors affecting demographic fluctuations during the Late Pleistocene, we used a diverse range of environmental factors, including annual temperature and precipitation during the Late Pleistocene (*63*). We collected elevation data from WorldDEM (*82*). Human disturbance data during the Late Pleistocene were from Timmermann *et al.* (*83*). The data were modeled using the human dispersal model considering changes in temperature, plant growth, desert size, and sea levels over time. This model was based on data from a large climate simulation covering the past 125,000 years and accurately recreating the scenarios of human migration during the Late Pleistocene. We aligned all environmental factors with the historical time periods of $N_e$.

To investigate the impacts of climate and human disturbance on SES-$N_e$ patterns in different Late Pleistocene periods, we performed spaMM analysis using the spaMM R package (table S3) (*84*).

## Supplementary Materials

**The PDF file includes:**

Figs. S1 to S34

Legends for tables S1 to S8

**Other Supplementary Material for this manuscript includes the following:**

Tables S1 to S8

## REFERENCES AND NOTES


1. C. N. Johnson, A. Balmford, B. W. Brook, J. C. Buettel, M. Galetti, L. Guangchun, J. M. Wilmshurst, Biodiversity losses and conservation responses in the Anthropocene. *Science* **356**, 270–275 (2017).
2. H.-O. Pörtner, R. J. Scholes, A. Arneth, D. K. A. Barnes, M. T. Burrows, S. E. Diamond, C. M. Duarte, W. Kiessling, P. Leadley, S. Managi, P. McElwee, G. Midgley, H. T. Ngo, D. Obura, U. Pascual, M. Sankaran, Y. J. Shin, A. L. Val, Overcoming the coupled climate and biodiversity crises and their societal impacts. *Science* **380**, eabl4881 (2023).
3. W. Zhou, M. Wang, M. Huang, F. Wei, A marine biodiversity plan for China and beyond. *Science* **371**, 685–686 (2021).
4. R. R. Germain, S. Feng, G. Chen, G. R. Graves, J. A. Tobias, C. Rahbek, F. Lei, J. Fjeldså, P. A. Hosner, M. T. P. Gilbert, G. Zhang, D. Nogués-Bravo, Species-specific traits mediate avian demographic responses under past climate change. *Nat. Ecol. Evol.* **7**, 862–872 (2023).
5. J. Wang, A. Caballero, Developments in predicting the effective size of subdivided populations. *Heredity* **82**, 212–226 (1999).
6. H. Li, R. Durbin, Inference of human population history from individual whole-genome sequences. *Nature* **475**, 493–496 (2011).
7. Y. Malhi, C. E. Doughty, M. Galetti, F. A. Smith, J.-C. Svenning, J. W. Terborgh, Megafauna and ecosystem function from the Pleistocene to the Anthropocene. *Proc. Natl. Acad. Sci. U.S.A.* **113**, 838–846 (2016).
8. A. Cooper, C. Turney, K. A. Hughen, B. W. Brook, H. G. McDonald, C. J. A. Bradshaw, Abrupt warming events drove Late Pleistocene Holarctic megafaunal turnover. *Science* **349**, 602–606 (2015).
9. J. R. Stewart, A. M. Lister, I. Barnes, L. Dalén, Refugia revisited: Individualistic responses of species in space and time. *Proc. R. Soc. B Biol. Sci.* **277**, 661–671 (2009).
10. S. Zhao, P. Zheng, S. Dong, X. Zhan, Q. Wu, X. Guo, Y. Hu, W. He, S. Zhang, W. Fan, L. Zhu, D. Li, X. Zhang, Q. Chen, H. Zhang, Z. Zhang, X. Jin, J. Zhang, H. Yang, J. Wang, J. Wang, F. Wei, Whole-genome sequencing of giant pandas provides insights into demographic history and local adaptation. *Nat. Genet.* **45**, 67–71 (2013).
11. Y. Hu, A. Thapa, H. Fan, T. Ma, Q. Wu, S. Ma, D. Zhang, B. Wang, M. Li, L. Yan, F. Wei, Genomic evidence for two phylogenetic species and long-term population bottlenecks in red pandas. *Sci. Adv.* **6**, eaax5751 (2020).
12. L. Yang, F. Wei, X. Zhan, H. Fan, P. Zhao, G. Huang, J. Chang, Y. Lei, Y. Hu, Evolutionary conservation genomics reveals recent speciation and local adaptation in threatened Takins. *Mol. Biol. Evol.* **39**, msac111 (2022).
13. J. Bergman, R. Ø. Pedersen, E. J. Lundgren, R. T. Lemoine, S. Monsarrat, E. A. Pearce, M. H. Schierup, J.-C. Svenning, Worldwide Late Pleistocene and Early Holocene population declines in extant megafauna are associated with *Homo sapiens* expansion rather than climate change. *Nat. Commun.* **14**, 7679 (2023).
14. W. Shichao, F. Huizhong, Z. Wenliang, H. Guangping, H. Yan, W. Shibao, W. Xiao, C. Yiting, T. Xinyue, W. Fuwen, Conservation genomics of the critically endangered Chinese pangolin. *Sci. China Life Sci.* **67**, 2051–2061 (2024).
15. C. R. Peart, S. Tusso, S. D. Pophaly, F. Botero-Castro, C.-C. Wu, D. Aurioles-Gamboa, A. B. Baird, J. W. Bickham, J. Forcada, F. Galimberti, N. J. Gemmell, J. I. Hoffman, K. M. Kovacs, M. Kunnasranta, C. Lydersen, T. Nyman, L. R. de Oliveira, A. J. Orr, S. Sanvito,

M. Valtonen, A. B. A. Shafer, J. B. W. Wolf, Determinants of genetic variation across eco-evolutionary scales in pinnipeds. *Nat. Ecol. Evol.* **4**, 1095–1104 (2020).
16. A. Higashino, R. Sakate, Y. Kameoka, I. Takahashi, M. Hirata, R. Tanuma, T. Masui, Y. Yasutomi, N. Osada, Whole-genome sequencing and analysis of the Malaysian cynomolgus macaque (*Macaca fascicularis*) genome. *Genome Biol.* **13**, R58 (2012).
17. J.-C. Svenning, R. T. Lemoine, J. Bergman, R. Buitenwerf, E. L. Roux, E. Lundgren, N. Mungi, R. Ø. Pedersen, The late-Quaternary megafauna extinctions: Patterns, causes, ecological consequences and implications for ecosystem management in the Anthropocene. *Camb. Prisms Extinct.* **2**, e5 (2024).
18. A. D. Foote, R. Hooper, A. Alexander, R. W. Baird, C. S. Baker, L. Ballance, J. Barlow, A. Brownlow, T. Collins, R. Constantine, L. Dalla Rosa, N. J. Davison, J. W. Durban, R. Esteban, L. Excoffier, S. L. F. Martin, K. A. Forney, T. Gerrodette, M. T. P. Gilbert, C. Guinet, M. B. Hanson, S. Li, M. D. Martin, K. M. Robertson, F. I. P. Samarra, R. de Stephanis, S. B. Tavares, P. Tixier, J. A. Totterdell, P. Wade, J. B. W. Wolf, G. Fan, Y. Zhang, P. A. Morin, Runs of homozygosity in killer whale genomes provide a global record of demographic histories. *Mol. Ecol.* **30**, 6162–6177 (2021).
19. D. J. Meltzer, Overkill, glacial history, and the extinction of North America's Ice Age megafauna. *Proc. Natl. Acad. Sci. U.S.A.* **117**, 28555–28563 (2020).
20. K. Nadachowska-Brzyska, C. Li, L. Smeds, G. Zhang, H. Ellegren, Temporal dynamics of avian populations during Pleistocene revealed by whole-genome sequences. *Curr. Biol.* **25**, 1375–1380 (2015).
21. M. Vellend, Conceptual synthesis in community ecology. *Q. Rev. Biol.* **85**, 183–206 (2010).
22. A. D. Barnosky, P. L. Koch, R. S. Feranec, S. L. Wing, A. B. Shabel, Assessing the causes of Late Pleistocene extinctions on the continents. *Science* **306**, 70–75 (2004).
23. J. M. Broughton, E. M. Weitzel, Population reconstructions for humans and megafauna suggest mixed causes for North American Pleistocene extinctions. *Nat. Commun.* **9**, 5441 (2018).
24. E. D. Lorenzen, D. Nogués-Bravo, L. Orlando, J. Weinstock, J. Binladen, K. A. Marske, A. Ugan, M. K. Borregaard, M. T. P. Gilbert, R. Nielsen, S. Y. W. Ho, T. Goebel, K. E. Graf, D. Byers, J. T. Stenderup, M. Rasmussen, P. F. Campos, J. A. Leonard, K.-P. Koepfli, D. Froese, G. Zazula, T. W. Stafford, K. Aaris-Sørensen, P. Batra, A. M. Haywood, J. S. Singarayer, P. J. Valdes, G. Boeskorov, J. A. Burns, S. P. Davydov, J. Haile, D. L. Jenkins, P. Kosintsev, T. Kuznetsova, X. Lai, L. D. Martin, H. G. McDonald, D. Mol, M. Meldgaard, K. Munch, E. Stephan, M. Sablin, R. S. Sommer, T. Sipko, E. Scott, M. A. Suchard, A. Tikhonov, R. Willerslev, R. K. Wayne, A. Cooper, M. Hofreiter, A. Sher, B. Shapiro, C. Rahbek, E. Willerslev, Species-specific responses of Late Quaternary megafauna to climate and humans. *Nature* **479**, 359–364 (2011).
25. J. Årevall, R. Early, A. Estrada, U. Wennergren, A. C. Eklöf, Conditions for successful range shifts under climate change: The role of species dispersal and landscape configuration. *Divers. Distrib.* **24**, 1598–1611 (2018).
26. R. Shine, Why is sex determined by nest temperature in many reptiles? *Trends Ecol. Evol.* **14**, 186–189 (1999).
27. S. I. Hayden Bofill, M. P. K. Blom, Climate change from an ectotherm perspective: Evolutionary consequences and demographic change in amphibian and reptilian populations. *Biodivers. Conserv.* **33**, 905–927 (2024).
28. A. R. Blaustein, S. C. Walls, B. A. Bancroft, J. J. Lawler, C. L. Searle, S. S. Gervasi, Direct and indirect effects of climate change on amphibian populations. *Diversity* **2**, 281–313 (2010).
29. F. Held, H. Cheng, R. L. Edwards, O. Tüysüz, K. Koç, D. Fleitmann, Dansgaard-Oeschger cycles of the penultimate and last glacial period recorded in stalagmites from Türkiye. *Nat. Commun.* **15**, 1183 (2024).
30. P. L. Koch, A. D. Barnosky, Late Quaternary extinctions: State of the debate. *Annu. Rev. Ecol. Evol. Syst.* **37**, 215–250 (2006).
31. M. A. Stoffel, E. Humble, A. J. Paijmans, K. Acevedo-Whitehouse, B. L. Chilvers, B. Dickerson, F. Galimberti, N. J. Gemmell, S. D. Goldsworthy, H. J. Nichols, O. Krüger, S. Negro, A. Osborne, T. Pastor, B. C. Robertson, S. Sanvito, J. K. Schultz, A. B. A. Shafer, J. B. W. Wolf, J. I. Hoffman, Demographic histories and genetic diversity across pinnipeds are shaped by human exploitation, ecology and life-history. *Nat. Commun.* **9**, 4836 (2018).
32. M. Huang, G. Huang, H. Fan, F. Wei, Influence of Last Glacial Maximum legacies on functional diversity and community assembly of extant Chinese terrestrial vertebrates. *Innovation* **4**, 100379 (2023).
33. J. F. Storz, U. Ramakrishnan, S. C. Alberts, Genetic effective size of a wild primate population: Influence of current and historical demography. *Evolution* **56**, 817–829 (2002).
34. N. Myers, R. A. Mittermeier, C. G. Mittermeier, G. A. B. da Fonseca, J. Kent, Biodiversity hotspots for conservation priorities. *Nature* **403**, 853–858 (2000).
35. S. J. E. Velazco, F. Villalobos, F. Galvão, P. De Marco Júnior, Transboundary conservation opportunities for Cerrado's plant species. *Biol. Conserv.* **284**, 110194 (2023).
36. S. A. Bhagwat, K. J. Willis, Species persistence in northerly glacial refugia of Europe: A matter of chance or biogeographical traits? *J. Biogeogr.* **35**, 464–482 (2008).
37. S. A. Zimov, N. S. Zimov, A. N. Tikhonov, F. S. Chapin III, Mammoth steppe: A high-productivity phenomenon. *Quat. Sci. Rev.* **57**, 26–45 (2012).
38. A. J. Monteath, B. V. Gaglioti, M. E. Edwards, D. Froese, Late Pleistocene shrub expansion preceded megafauna turnover and extinctions in eastern Beringia. *Proc. Natl. Acad. Sci. U.S.A.* **118**, e2107977118 (2021).
39. S. C. Brown, T. M. L. Wigley, B. L. Otto-Bliesner, C. Rahbek, D. A. Fordham, Persistent Quaternary climate refugia are hospices for biodiversity in the Anthropocene. *Nat. Clim. Change* **10**, 244–248 (2020).
40. K. Lambeck, J. Chappell, Sea level change through the last glacial cycle. *Science* **292**, 679–686 (2001).
41. M. B. Araújo, F. Ferri-Yáñez, F. Bozinovic, P. A. Marquet, F. Valladares, S. L. Chown, Heat freezes niche evolution. *Ecol. Lett.* **16**, 1206–1219 (2013).
42. M. Dehasque, H. E. Morales, D. Díez-del-Molino, P. Pečnerová, J. C. Chacón-Duque, F. Kanellidou, H. Muller, V. Plotnikov, A. Protopopov, A. Tikhonov, P. Nikolskiy, G. K. Danilov, M. Giannì, L. van der Sluis, T. Higham, P. D. Heintzman, N. Oskolkov, M. T. P. Gilbert, A. Götherström, T. van der Valk, S. Vartanyan, L. Dalén, Temporal dynamics of woolly mammoth genome erosion prior to extinction. *Cell* **187**, 3531–3540.e13 (2024).
43. E. Palkopoulou, S. Mallick, P. Skoglund, J. Enk, N. Rohland, H. Li, A. Omrak, S. Vartanyan, H. Poinar, A. Götherström, D. Reich, L. Dalén, Complete genomes reveal signatures of demographic and genetic declines in the woolly mammoth. *Curr. Biol.* **25**, 1395–1400 (2015).
44. A. J. Stuart, P. A. Kosintsev, T. F. G. Higham, A. M. Lister, Pleistocene to Holocene extinction dynamics in giant deer and woolly mammoth. *Nature* **431**, 684–689 (2004).
45. M. I. Bird, L. B. Hutley, M. J. Lawes, J. Lloyd, J. G. Luly, P. V. Ridd, R. G. Roberts, S. Ulm, C. M. Wurster, Humans, megafauna and environmental change in tropical Australia. *J. Quat. Sci.* **28**, 439–452 (2013).
46. A. J. Stuart, Late Quaternary megafaunal extinctions on the continents: A short review. *Geol. J.* **50**, 338–363 (2015).
47. M. A. Supple, B. Shapiro, Conservation of biodiversity in the genomics era. *Genome Biol.* **19**, 131 (2018).
48. C. Zhang, Y. Li, X. Hu, X. Ma, W. Jia, K. Liu, Y. Nie, Human-induced behavioural changes of global threatened terrestrial mammals. *Glob. Ecol. Biogeogr.* **32**, 1645–1659 (2023).
49. W. Rodríguez, O. Mazet, S. Grusea, A. Arredondo, J. M. Corujo, S. Boitard, L. Chikhi, The IICR and the non-stationary structured coalescent: Towards demographic inference with arbitrary changes in population structure. *Heredity* **121**, 663–678 (2018).
50. H. Teixeira, J. Salmona, A. Arredondo, B. Mourato, S. Manzi, R. Rakotondravony, O. Mazet, L. Chikhi, J. Metzger, U. Radespiel, Impact of model assumptions on demographic inferences: The case study of two sympatric mouse lemurs in northwestern Madagascar. *BMC Ecol. Evol.* **21**, 197 (2021).
51. O. Mazet, W. Rodríguez, S. Grusea, S. Boitard, L. Chikhi, On the importance of being structured: Instantaneous coalescence rates and human evolution—Lessons for ancestral population size inference? *Heredity* **116**, 362–371 (2016).
52. L. Chikhi, W. Rodriguez, S. Grusea, P. Santos, S. Boitard, O. Mazet, The IICR (inverse instantaneous coalescence rate) as a summary of genomic diversity: Insights into demographic inference and model choice. *Heredity* **120**, 13–24 (2018).
53. M. Nordborg, B. Charlesworth, D. Charlesworth, The effect of recombination on background selection. *Genet. Res.* **67**, 159–174 (1996).
54. T. Cousins, A. Scally, R. Durbin, A structured coalescent model reveals deep ancestral structure shared by all modern humans. *Nat. Genet.* **57**, 856–864 (2025).
55. H. Li, Protein-to-genome alignment with miniprot. *Bioinformatics* **39**, btad014 (2023).
56. R. C. Edgar, MUSCLE: Multiple sequence alignment with high accuracy and high throughput. *Nucleic Acids Res.* **32**, 1792–1797 (2004).
57. S. Capella-Gutiérrez, J. M. Silla-Martínez, T. Gabaldón, trimAl: A tool for automated alignment trimming in large-scale phylogenetic analyses. *Bioinformatics* **25**, 1972–1973 (2009).
58. A. Stamatakis, RAxML version 8: A tool for phylogenetic analysis and post-analysis of large phylogenies. *Bioinformatics* **30**, 1312–1313 (2014).
59. M. J. Sanderson, r8s: Inferring absolute rates of molecular evolution and divergence times in the absence of a molecular clock. *Bioinformatics* **19**, 301–302 (2003).
60. S. M. Kiełbasa, R. Wan, K. Sato, P. Horton, M. C. Frith, Adaptive seeds tame genomic sequence comparison. *Genome Res.* **21**, 487–493 (2011).
61. M. Blanchette, W. J. Kent, C. Riemer, L. Elnitski, A. F. A. Smit, K. M. Roskin, R. Baertsch, K. Rosenbloom, H. Clawson, E. D. Green, D. Haussler, W. Miller, Aligning multiple genomic sequences with the threaded blockset aligner. *Genome Res.* **14**, 708–715 (2004).
62. A. Zizka, D. Silvestro, T. Andermann, J. Azevedo, C. Duarte Ritter, D. Edler, H. Farooq, A. Herdean, M. Ariza, R. Scharn, S. Svantesson, N. Wengström, V. Zizka, A. Antonelli, CoordinateCleaner: Standardized cleaning of occurrence records from biological collection databases. *Methods Ecol. Evol.* **10**, 744–751 (2019).
63. R. M. Beyer, M. Krapp, A. Manica, High-resolution terrestrial climate, bioclimate and vegetation for the last 120,000 years. *Sci. Data* **7**, 236 (2020).
64. S. Chen, Y. Zhou, Y. Chen, J. Gu, fastp: An ultra-fast all-in-one FASTQ preprocessor. *Bioinformatics* **34**, i884–i890 (2018).
65. H. Li, R. Durbin, Fast and accurate short read alignment with Burrows–Wheeler transform. *Bioinformatics* **25**, 1754–1760 (2009).

66. W. Thuiller, M. Guéguen, J. Renaud, D. N. Karger, N. E. Zimmermann, Uncertainty in ensembles of global biodiversity scenarios. *Nat. Commun.* **10**, 1446 (2019).
67. M. Barbet-Massin, W. Jetz, The effect of range changes on the functional turnover, structure and diversity of bird assemblages under future climate scenarios. *Glob. Chang. Biol.* **21**, 2917–2928 (2015).
68. W. Thuiller, D. Georges, M. Gueguen, R. Engler, F. Breiner, B. Lafourcade, R. Patin, biomod2: Ensemble platform for species distribution modeling, version 4.2-3, CRAN (2023); https://cran.r-project.org/web/packages/biomod2/index.html.
69. O. Allouche, A. Tsoar, R. Kadmon, Assessing the accuracy of species distribution models: Prevalence, kappa and the true skill statistic (TSS). *J. Appl. Ecol.* **43**, 1223–1232 (2006).
70. E. J. Pedersen, D. L. Miller, G. L. Simpson, N. Ross, Hierarchical generalized additive models in ecology: An introduction with mgcv. *PeerJ* **7**, e6876 (2019).
71. G. L. Simpson, H. Singmann, gratia: graceful 'ggplot'-based graphics and other functions for GAMs fitted using "mgcv", version 0.10.0, CRAN (2024); https://cran.r-project.org/web/packages/gratia/index.html.
72. F. Sayol, M. J. Steinbauer, T. M. Blackburn, A. Antonelli, S. Faurby, Anthropogenic extinctions conceal widespread evolution of flightlessness in birds. *Sci. Adv.* **6**, eabb6095 (2020).
73. C. Sheard, M. H. C. Neate-Clegg, N. Alioravainen, S. E. I. Jones, C. Vincent, H. E. A. MacGregor, T. P. Bregman, S. Claramunt, J. A. Tobias, Ecological drivers of global gradients in avian dispersal inferred from wing morphology. *Nat. Commun.* **11**, 2463 (2020).
74. J. Staerk, D. A. Conde, V. Ronget, J.-F. Lemaitre, J.-M. Gaillard, F. Colchero, Performance of generation time approximations for extinction risk assessments. *J. Appl. Ecol.* **56**, 1436–1446 (2019).
75. L. A. Bergeron, S. Besenbacher, J. Zheng, P. Li, M. F. Bertelsen, B. Quintard, J. I. Hoffman, Z. Li, J. St. Leger, C. Shao, J. Stiller, M. T. P. Gilbert, M. H. Schierup, G. Zhang, Evolution of the germline mutation rate across vertebrates. *Nature* **615**, 285–291 (2023).
76. S. Aghabozorgi, A. Seyed Shirkhorshidi, T. Ying Wah, Time-series clustering – A decade review. *Inf. Syst.* **53**, 16–38 (2015).
77. A. Sarda-Espinosa, dtwclust: Time series clustering along with optimizations for the dynamic time warping distance, version 5.5.12, CRAN (2023); https://cran.r-project.org/web/packages/dtwclust/index.html.
78. T. Galili, dendextend: An R package for visualizing, adjusting and comparing trees of hierarchical clustering. *Bioinformatics* **31**, 3718–3720 (2015).
79. Y. Hu, H. Fan, Y. Chen, J. Chang, X. Zhan, H. Wu, B. Zhang, M. Wang, W. Zhang, L. Yang, X. Hou, X. Shen, T. Pan, W. Wu, J. Li, H. Hu, F. Wei, Spatial patterns and conservation of genetic and phylogenetic diversity of wildlife in China. *Sci. Adv.* **7**, eabd5725 (2021).
80. S. W. Kembel, P. D. Cowan, M. R. Helmus, W. K. Cornwell, H. Morlon, D. D. Ackerly, S. P. Blomberg, C. O. Webb, Picante: R tools for integrating phylogenies and ecology. *Bioinformatics* **26**, 1463–1464 (2010).
81. L. Kuczynski, V. J. Ontiveros, H. Hillebrand, Biodiversity time series are biased towards increasing species richness in changing environments. *Nat. Ecol. Evol.* **7**, 994–1001 (2023).
82. G. Riegler, S. D. Hennig, M. Weber, WorldDEM – A novel global foundation layer. *Int. Arch. Photogramm. Remote Sens. Spat. Inf. Sci.* **40**, 183–187 (2015).
83. A. Timmermann, T. Friedrich, Late Pleistocene climate drivers of early human migration. *Nature* **538**, 92–95 (2016).
84. F. Rousset, J. B. Ferdy, Testing environmental and genetic effects in the presence of spatial autocorrelation. *Ecography* **37**, 781–790 (2014).
85. B. G. Holt, J.-P. Lessard, M. K. Borregaard, S. A. Fritz, M. B. Araújo, D. Dimitrov, P.-H. Fabre, C. H. Graham, G. R. Graves, K. A. Jønsson, D. Nogués-Bravo, Z. Wang, R. J. Whittaker, J. Fjeldså, C. Rahbek, An update of Wallace's zoogeographic regions of the world. *Science* **339**, 74–78 (2013).

**Acknowledgments:** We thank E. I. Ameca, M. Huang, and X. Huang for discussions about paper writing. We thank M. Wang and D. Guan for assistance in this study. **Funding:** This work was supported by the following grants: the National Key Program of Research and Development of Ministry of Science and Technology, 2023YFF1304800 (to H.F.); the National Natural Science Foundation of China, grant nos. 31821001 (to F.W.) and 32201424 (to Z. Lia.); and Major Program of the Natural Science Foundation of Jiangxi Province of China, 20233ACB209001 (to F.W.). **Author contributions:** Conceptualization, methodology, software, visualization, formal analysis, writing—original draft, writing—review and editing, validation: Z. Lia., and F.W. Investigation: Z. Li, H.F., Y.W., and F.W. Supervision and project administration: Z. Li, H.F., and F.W. Resources and data curation: Z. Li and F.W. Funding acquisition: H.F., Z. Lia., and F.W. **Competing interests:** The authors declare that they have no competing interests. **Data and materials availability:** All data needed to evaluate the conclusions in the paper are present in the paper and/or the Supplementary Materials. The GenBank accession IDs of all reused genomes in the study have been listed in table S1. The data and scripts used to make for this study are available in Dryad (https://doi.org/10.5061/dryad.31zcrjdwq).

Submitted 11 May 2024
Accepted 22 April 2025
Published 23 May 2025
10.1126/sciadv.adq3938